Strain-based joint damage estimation approach robust to unknown non-stationary input force

Neha Aswal, Subhamoy Sen, Laurent Mevel

Strain-based joint damage estimation approach robust to unknown non-stationary input force

Neha Aswal[a], Subhamoy Sen[a,*], Laurent Mevel[b]

[a] *Indian Institute of Technology Mandi, Mandi, HP, India*
[b] *Univ. Gustave Eiffel, Inria, Cosys-SII, I4S, Campus de Beaulieu, Rennes, France*

Abstract

To avert catastrophic failure in the structures, joints are typically designed to yield, but not fail, so that energy accumulated under cyclic loading is dissipated. Eventually, this renders the structural joints to be characteristically weaker and more vulnerable than the members. Yet, damage detection research mostly assumes damage in the members only. This article proposes a model-based predictor-corrector algorithm that uses an interacting filtering approach to efficiently estimate joint damage in the presence of input and measurement uncertainties. For the predictor model, a novel strain-displacement relationship specific to semi-rigid frames is developed to map nodal displacements to corresponding strain measurements. The proposed estimation method embeds robustness against non-stationary input (e.g. seismic excitation) in the state filter, itself. For this, an output injection technique is integrated within the state filter. The modified state filter (robust Kalman filter) runs within an enveloping parameter filter (Particle filter) to simultaneously estimate the system states and joint damage parameters, respectively, using the response signal. Strain has been adopted as measurement since it is frame independent (beneficial for seismic activity) and also comparatively cheaper to use. Numerical studies are performed on a two-dimensional three story-three bay shear frame for different joint damage locations and severities. The sensitivity and the stability of the proposed approach are further investigated. Experimental validation of the proposed algorithm is carried out on a 2-D steel frame.

1. Introduction

Structural joints ensure efficient load transfer mechanism between the connected members. A damage in a joint may therefore jeopardize the structural integrity. While in reinforced concrete structures, joints mostly fail due to crushing of concrete and/or yielding of reinforcements, damage in steel structural joints are mostly due to yielding and cracking in bolts or brackets. Under prolonged cyclic loading, the threaded bolts may also get loosened, affecting the joint stiffness. Especially for the steel structures, damage in joint is

*Corresponding author; *E-mail address: subhamoy@iitmandi.ac.in*

observed to be more frequent than member failure [1, 2]. This is due to the design philosophy that ascertains the joints to fail before the members. Since damage in joints dissipates the energy accumulated under a severe load, a weaker joint design, in turn, safeguards the members, avoiding human casualty. However, an undetected joint damage may further propagate, leading to either a complete disengagement of the connected members or a disruption of structural stability, resulting in damage in the members as well.

Researches in structural health monitoring (SHM), however, have mostly considered damage in the structural members [3–6], except for a few cases where damage in the joints have also been taken into account [1, 2, 7–9]. In the design or the modeling phase, joints are typically categorized as either fixed or pinned depending on the assumption on their moment transfer property, i.e., joints assumed with infinite or zero rotational stiffness, respectively. Accordingly, typical SHM approaches also follow this idealization. However, in reality, the joints can be categorized as something in between these two extremes. This joint definition is typically termed as semi-rigid connections, i.e., they neither transfer the moment completely nor behave like moment-free pins. Without incorporating this semi-rigid definition in the model, it is difficult for a model-based damage detection approach to identify any intermediate damaged stage for joints.

Model-independent non-destructive testing techniques [10–12] exist for joint damage detection which necessitate the testing to be done in the vicinity of the damage location, calling for dense and therefore costly instrumentation. Alternatively, data-based approaches [7, 13, 14] are also reported which detect and localize joint damage without quantifying the severity. Several other studies have employed deterministic approaches in time [8] or modal domain [1, 9] in order to quantify the severity of the structural damage. Since the system under consideration is subjected to unknown input force and the available measurements are contaminated with uncertain noise, a deterministic approach can not be an ideal approach.

The majority of the reported approaches for joint damage assessment are deterministic, lacking focus on the uncertainties involved in the real field applications. In reality, uncertainties can originate from model inaccuracies, sensor noise, as well as unknown external disturbances, or outliers in data. In fact, none of these uncertainties can be alleviated or ignored but can be modeled using certain statistical models. With the Bayesian filtering-based stochastic estimation approach, the system can be estimated efficiently even in the presence of system and measurement uncertainties as long as the uncertainty models are available. Successful application of this approach for SHM problems has been reported in abundance [15–21].

General Bayesian estimation defines the system dynamics with a set of unobserved states observed through a set of measurements. The approach further involves two recursive procedures: (i) propagation of state estimate in time using Chapman-Kolmogorov equation, and (ii) a minimum mean square error (MMSE) based correction of the propagated state estimates using recorded measurements. In the context of SHM, the Chapman-Kolmogorov equation is a probabilistic state space model of the process dynamics which incorporates the associated process uncertainties that arise due to forces and external disturbances. To further estimate damage in the structures, damage indices of concern are augmented in the state definition

to estimate them in time, alongside the states [22–24].

Estimating parameters as augmented states have many a times been observed to cause a divergence in the solution, yielding a false or unfeasible solution especially for time-varying systems [25]. Dimensional augmentation of the states with damage indices has also been experienced to be computationally unmanageable and expensive. Moreover, while the propagation of regular system states may or may not be linear, the parameter estimation is always a nonlinear problem because of the nonlinear mapping of the parameters to the corresponding measurements. Thus, combining a nonlinear estimation problem with a linear one is not always an economically viable option. Employing separate filters for states and parameters and exchanging information through interaction has proved to be a more efficient alternative. Thus states and parameters are estimated through mutual conditioning (also called Rao-Blackwellisation [18, 19, 26–29]) that helps to maintain the state dimensions within manageable dimension while ensuring stability in estimation. The relative potential of interactive estimation over joint estimation technique in the context of computational economy and stability has been corroborated in [30].

Nonlinear filter variants (e.g., Extended (EKF) [31] /Unscented (UKF) [32, 33]/Ensemble (EnKF) variant of KF, Particle filter, etc.) are required to handle nonlinear parameter estimation problems. Particle filter (PF) [34, 35], is known as a robust approach in this endeavor [22, 36, 37]. Implementation of PF has concerns over its computational expense [38] and is therefore advisable as long as the parameter dimensions are manageable. A modified nonlinear observer, i.e., extended model-based observer (EMBO) has also been introduced to estimate states in hysteretic nonlinear structural systems [39] by modifying nonlinear finite element predictor model. Validated on large scale structures, methods based on modification of the state model [39, 40], to estimate states and identify structural damage, have shown potential in SHM of real-life structure. However, since the methods are frequency-based, they may not be suitable for real-time SHM application.

Following the marginalization approach introduced by [41],[42] proposed Interacting Particle-Kalman filter (IPKF) that combines PF, for parameter estimation, with KF for linear state estimation problem. This approach has further been improved for computational efficiency by [43] and for a system with correlated noise by [44]. This approach assumes stationarity and Gaussianity for input forcing which most often gets violated, especially for the cases with wind/wave/seismic excitation. An improved version of the mentioned IPKF algorithm includes an additional force filter to handle non-stationary forcing types [18], which also increases the computational time. There are studies that focus on input force estimation filters [45, 46] for time varying systems with input as an additional state [47–51]. Explicit proofs of stability and observability for similar filters are also investigated in detail [52, 53]. Augmentation of the inputs in the state vector sometimes may however cause an intractable integration [25] jeopardizing the estimation. The solution for this is to make the estimation robust to input, so that the need to estimate the input can be outrightly avoided. To achieve this, output injection approach introduced by [54] is integrated within the IPKF

environment that rejects the unknown inputs by simply transforming the system model, so that state and/or parameter estimation algorithms can be applied as if the rejected unknown inputs no longer exist. This noise robust filtering approach is extended to Ensemble Kalman Filter (r-EnKF) in [55], which is however computationally expensive since a good amount of state ensembles are required to be propagated in each time update. For the considered case of linear dynamics, a computationally lighter state estimation through Kalman filtering is preferred. Accordingly this paper presents the first embedding of such approach into IPKF, wherein the structural parameters of a linear system are monitored under an unknown ambient excitation.

Such model-based approaches require efficient models to infer the interrelation between a damage in any semi-rigid connection and its signature in the measured responses. Thankfully, a significant amount of work on this topic has been done in recent studies [1, 20, 56], which can be taken as a basis. The required measurement model to predict strain through a linear mapping of nodal motion, has been developed accordingly. The associated strain-displacement relationship (and also interpolating the nodal response values through the spatial derivatives of analytical shape-function for strain mapping) has been derived in the form that can be directly used for estimating a system defined in state-space.

Moreover, since joint damage mostly occurs under severe loading conditions, the proposed algorithm is expected to be robust against uncertain inputs, e.g. cyclic loading, seismic base excitation, etc. Cyclic load may cause temporary nonlinear behaviour in the structural response which is typically considered in forward modelling approach for better replication requirement [57]. Nevertheless, within a stochastic inverse estimation environment, incorporation of such detailed dynamics in the predictor model demanding recursive simulation will lead to exorbitant increase in the computational cost. With Bayesian filtering approaches, such minor inaccuracies can be modelled as process uncertainty. Thus, even if the model is lacking the exact replicability with respect to real structural phenomena, it can still be useful with Bayesian filtering approaches in its recursive estimation approach.

Under base excitation, the acceleration responses, collected from accelerometers patched on to the structure, are not pertinent since acceleration measurements are not independent of the frame of reference. To achieve frame independence in the measurement, present study employs strain as the measurement. Further, the acceleration sensors are costly and their placement on the nodes (structural joints) are not always easy due to the accessibility reasons. Also strain responses are better damage sensitive features and therefore suitable for detecting weaker damage, such as joint damage.

Typical approaches of defining state space dynamics of mechanical systems using displacement and velocity (as states) require a detailed model for strain mapping from nodal displacements, rendering the entire approach to be compute-intensive. In this article, strain has been mapped using interpolation (/shape) functions to predict strain at specified member locations with respect to the joint stiffness indices of the joints connecting the member, which may seem crude compared to a detailed modeling approach. However, with

Bayesian filtering approach, the relative modeling inaccuracies can always be circumvented by assuming additional process noise and using recursive estimation approach. Therefore, this crude strain mapping strategy may in turn lead to a practical, time-saving and cost-effective estimation of structural health. While mapping of dynamic strain from nodal response of an Euler-Bernoulli beam is a well known approach, the same is not true for beam element with semi-rigid connections. Although procedural, the mapping of dynamic strain from nodal response of a beam element with semi-rigid connections has not been discussed in the existing literature, and therefore has also been taken up in this study.

The current proposal employs interacting filtering strategy for joint damage detection that amalgamates the real time input robust detection capability of an interacting filtering approach with a dynamic model of a semi-rigid frame defined in state space with simpler linear process and measurement model (which utilizes strain response). Such linear models inherently reduce the computational time attribute of the developed algorithm. The following sections give details of system modelling (for predictor model) and system estimation, i.e., r-IPKF. The proposed algorithm is further tested on a numerical two-dimensional three story-three bay shear frame for its accuracy, promptness and precision in joint damage detection, which is followed by an experimental validation study on a 2-D steel frame.

2. Problem definition and modeling

Being a Bayesian filtering-based predictor-corrector approach, the proposed method requires a fairly accurate system model replicating the reality. To achieve better predictive ability with a minimum increase in computational cost, the current study incorporates a semi-rigid joint model in the system modeling. In the following, the adopted modeling strategy is discussed followed by a detailed description of the proposed robust interacting filtering strategy.

2.1. Dynamics of beam with semi rigid joints

The governing differential equation for a typical linear time varying (LTV) mechanical system can be represented as,

$$\mathbf{M}(t)\ddot{\mathbf{q}}(t) + \mathbf{C}(t)\dot{\mathbf{q}}(t) + \mathbf{K}(t)\mathbf{q}(t) = \bar{\mathbf{w}}(t) - \mathbf{M}(t)\tau\ddot{\mathbf{a}}^{g}(t) \tag{1}$$

where $\mathbf{M}(t)$, $\mathbf{K}(t)$ and $\mathbf{C}(t)$ are $(n \times n)$ order mass, stiffness and damping matrices of the system, respectively, with n being the total degrees of freedom (*dof*s). The time variation of these system matrices is due to their dependence on the time varying joint stiffness index $\gamma(t)$. $\ddot{\mathbf{q}}(t)$, $\dot{\mathbf{q}}(t)$ and $\mathbf{q}(t)$ are the system's acceleration, velocity, and displacement responses, respectively. $\bar{\mathbf{w}}(t)$ is the unknown external ambient force acting on the structure. $\ddot{\mathbf{a}}^{g}(t)$ is the ground acceleration and τ is the location matrix that maps the effect of ground excitation to each of the nodes of the system.

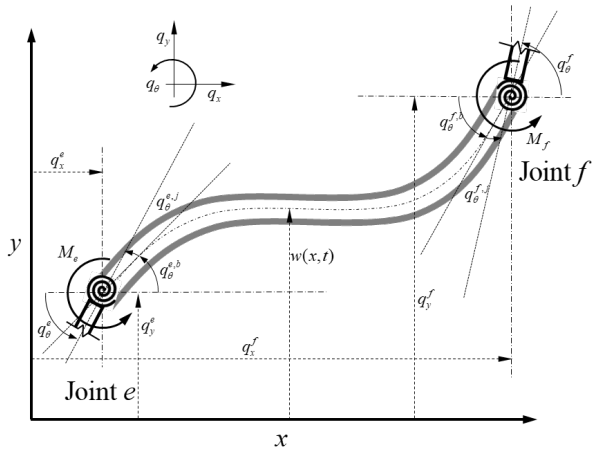

Figure 1: Schematic diagram of a beam element with semi-rigid joints.

The global stiffness/mass matrices are obtained through assembling elemental stiffness/mass matrices modeled using finite element modeling approach with the frame members idealized as semi-rigid beam elements (see schematic in Figure 1). The detailed element stiffness and mass matrix formulations are given in the Appendix A. It should be noted here that, unlike for the typical Euler-Bernoulli beams, the current mass matrix depends on the joint stiffness and is therefore assumed to be time-varying. Rayleigh's damping model has been used to compute $\mathbf{C}(t)$, which is also time-varying because of its dependence on $\mathbf{M}(t)$ and $\mathbf{K}(t)$. It should be noted that connection damping [58] is typically considered to mimic energy dissipation in joints in forward simulation models of semi-rigid frames targeting better replication of their seismic performance. However, for inverse estimation approaches this aspect can be ignored and the incurred modelling inaccuracies can be considered within process uncertainty. Thereby, even though this deteriorates the estimation precision, the estimation mean can always be expected to be unbiased with respect to the corresponding true values. This strategy helps to render the predictor model simpler and computationally inexpensive leading to faster computation.

2.2. Mapping of nodal displacements to strain

The present study adopts strain data as the only structural response to be obtained, from which the damage present in the joints is identified. For this, a predictor model is required that can map the displacement/velocity responses to the corresponding strain measures. The developed model takes basis on a strain-displacement relation of the Euler-Bernoulli beam supported on semi-rigid joints. The strain-displacement relation depends on the adopted shape functions specific to the selection of the element type.

For typical Euler-Bernoulli type beam elements (as shown in Figure 1 without the end springs), the associated shape functions are

$$\psi_1(\eta) = \frac{1}{4}(1-\eta)^2(2+\eta); \quad \psi_2(\eta) = \frac{l_m}{8}(1-\eta)^2(1+\eta)$$
$$\psi_3(\eta) = \frac{1}{4}(1+\eta)^2(2-\eta); \quad \psi_4(\eta) = \frac{l_m}{8}(1+\eta)^2(\eta-1) \tag{2}$$

with $\eta = 2x/l_m - 1$ and l_m being the length of the member. With these shape functions, the beam deflection due to bending can further be expressed as

$$w^b_{ef}(x,t) = \psi^b(\eta)\mathbf{q}^l_{ef}(t) \tag{3}$$

where $\psi^b(\eta) = [\psi_1(\eta) \quad \psi_2(\eta) \quad \psi_3(\eta) \quad \psi_4(\eta)]$. $\mathbf{q}^l_{ef}$ is the nodal displacement of the beam supported on joints e and f defined in LCS and can be expanded as: $\mathbf{q}^l_{ef} = \begin{bmatrix}\mathbf{q}^e_y & \mathbf{q}^e_\theta & \mathbf{q}^f_y & \mathbf{q}^f_\theta\end{bmatrix}$. The associated GCS displacements are $\mathbf{q}_{ef} = \begin{bmatrix}\mathbf{q}^e_X & \mathbf{q}^e_Y & \mathbf{q}^e_\Theta & \mathbf{q}^f_X & \mathbf{q}^f_Y & \mathbf{q}^f_\Theta\end{bmatrix}$. The transformation from LCS to GCS is achieved through a transformation matrix $\mathbf{T}$ as: $\mathbf{q}^l_{ef} = \mathbf{T}\mathbf{q}_{ef}$. Further two separate sets have been made out of $\mathbf{q}_{ef}$, as $\mathbf{q}^b = \begin{bmatrix}\mathbf{q}^e_Y & \mathbf{q}^e_\Theta & \mathbf{q}^f_Y & \mathbf{q}^f_\Theta\end{bmatrix}$ and $\mathbf{q}^a = \begin{bmatrix}\mathbf{q}^e_X & \mathbf{q}^f_X\end{bmatrix}$, which are individually responsible for the deflection due to bending and the axial deformation.

However, for beams with semi-rigid connections, the shape functions are the functions of joint stiffness, for which Equation 3 needs to be modified as,

$$\begin{Bmatrix} w^b(x,t) \\ w^a(x,t) \end{Bmatrix} = \begin{Bmatrix} \bar{\psi}^b(\eta)\mathbf{q}^b(t) \\ \bar{\psi}^a(\eta)\mathbf{q}^a(t) \end{Bmatrix} \tag{4}$$

where, $w^b(x,t)$ and $w^a(x,t)$ are the beam deflections due to beam and truss actions. $\bar{\psi}^b(\eta) = \psi^b(\eta)\left(\mathbf{I} - \frac{1}{\Delta}\mathbf{B}\right)$, $\bar{\psi}^a(\eta) = [-1/l_m \quad 1/l_m]$. $\bar{\psi}^b(\eta)$ can further be expanded as $\bar{\psi}^b(\eta) = \begin{bmatrix}\bar{\psi}_1(\eta) & \bar{\psi}_2(\eta) & \bar{\psi}_3(\eta) & \bar{\psi}_4(\eta)\end{bmatrix}$ with,

$$\bar{\psi}_1(\eta) = \psi_1 - c_1\psi_2 - c_2\psi_4; \quad \bar{\psi}_2(\eta) = (1-c_3)\psi_2 - c_4\psi_4;$$
$$\bar{\psi}_3(\eta) = \psi_3 + c_1\psi_2 + c_2\psi_4; \quad \bar{\psi}_4(\eta) = c_5\psi_2 + (1-c_6)\psi_4 \tag{5}$$

where $c_1 = \frac{6}{\Delta l_m}(W_e + 2W_eW_f)$, $c_2 = \frac{6}{\Delta l_m}(W_f + 2W_eW_f)$, $c_3 = \frac{4}{\Delta}(W_e + 3W_eW_f)$, $c_4 = \frac{2}{\Delta}W_f$, $c_5 = 2W_e$ and $c_6 = \frac{4}{\Delta}(W_f + 3W_eW_f)$. $\Delta = [(1+4W_e)(1+4W_f) - 4W_eW_f]$. W_e and W_f are the measures of flexibility of j^{th} joint and can be obtained as $W_j = 1/\gamma_j$. B can be obtained as

$$B = \begin{bmatrix} 0 & 0 & 0 & 0 \\ \frac{-6}{l_m}(W_e + 2W_eW_f) & -4(W_e + 3W_eW_f) & \frac{6}{l_m}(W_e + 2W_eW_f) & -2W_e \\ 0 & 0 & 0 & 0 \\ \frac{-6}{l_m}(W_f + 2W_eW_f) & -2W_e & \frac{6}{l_m}(W_e + 2W_eW_f) & -4(W_f + 3W_eW_f) \end{bmatrix} \tag{6}$$

Clearly, these shape functions depend on the joint stiffness index γ and hence are not the same for the damaged/undamaged system or even for systems with different joint damage severity. Strain estimation from

measured displacement data for structures with semi-rigid joints therefore requires a recursive calculation of the corresponding mode shapes. The slope $\theta^b(x,t)$ and curvature $\kappa^b(x,t)$ at an arbitrary point x at time t can be calculated as

$$\begin{aligned} \theta^b(x,t) = w^{b'}(x,t) &= \frac{\partial \bar{\psi}(\eta)}{\partial \eta}\frac{\partial \eta}{\partial x}\mathbf{q}^b(t) = \bar{\psi}^b_\theta(\eta)\mathbf{q}^b(t) \\ \kappa^b(x,t) = w^{b''}(x,t) &= \left(\frac{\partial^2 \bar{\psi}(\eta)}{\partial \eta^2}\left(\frac{\partial \eta}{\partial x}\right)^2 + \frac{\partial \bar{\psi}(\eta)}{\partial \eta}\frac{\partial^2 \eta}{\partial x^2}\right)\mathbf{q}^b(t) = \bar{\psi}^b_\kappa(\eta)\mathbf{q}^b(t) \end{aligned} \tag{7}$$

where shape function for slope and curvature can collectively be defined as $\bar{\psi}^b_{\kappa/\theta} = \left[\bar{\psi}^b_{\kappa/\theta,1}\ \bar{\psi}^b_{\kappa/\theta,2}\ \bar{\psi}^b_{\kappa/\theta,3}\ \bar{\psi}^b_{\kappa/\theta,4}\right]$.

The strain gauges are assumed here as patched on the bottom surface of the beam at its centre where strain is caused by bending (beam action) as well as axial deformation (truss action) in the beam. Thus strain along beam orientation (i.e., XX) of member ef can be obtained as

$$\begin{aligned} \varepsilon_{XX,ef}(x,t) &= \left[\bar{\psi}^a(\eta)\mathbf{q}^a(t)\right]_{axial} - \left[y\kappa^b(x,t)\right]_{bending} \\ &= \bar{\psi}^a(\eta)\mathbf{q}^a(t) - y\bar{\psi}^b_\kappa(\eta)\mathbf{q}^b(t) \end{aligned} \tag{8}$$

y is the depth of the extreme fibre at which the strain gauge is patched. Considering the strain gauges are patched on the bottom surface (at a distance d' from neutral axis) at middle point of the member, the strain displacement for any arbitrary member can finally be presented as

$$\varepsilon_{XX} = \left[-1/l_m \quad d'\bar{\psi}^b_{\kappa,1} \quad d'\bar{\psi}^b_{\kappa,2} \quad 1/l_m \quad d'\bar{\psi}^b_{\kappa,3} \quad d'\bar{\psi}^b_{\kappa,4}\right]\mathbf{q}^l_{ef}(t) = \Psi\mathbf{q}^l_{ef}(t) \tag{9}$$

2.3. State space formulation for the system dynamics

Bayesian filtering technique is employed in this article to estimate joint stiffness index. For this, the system dynamics has been defined in state space and a measurement equation that connects the unobserved states to the corresponding measurements, has also been set up.

Let $\mathbf{F}(t) = \begin{bmatrix} \mathbf{0}_n & \mathbf{I}_n \\ -\mathbf{M}(t)^{-1}\mathbf{K}(t) & -\mathbf{M}(t)^{-1}\mathbf{C}(t) \end{bmatrix}_{2n\times 2n}$, $\mathbf{B}_c(t) = \begin{bmatrix} \mathbf{0}_n \\ \mathbf{M}(t)^{-1} \end{bmatrix}_{2n\times m}$, $\mathbf{E}_c = \begin{bmatrix} \mathbf{0} \\ -\tau \end{bmatrix}_{2n\times l}$ and $\mathbf{x}(t) = \left[\mathbf{q}^T(t) \quad \dot{\mathbf{q}}^T(t)\right]^T_{2n\times 1}$, the system dynamics, given in Equation 1, can be described in its continuous time as,

$$\dot{\mathbf{x}}(t) = \mathbf{F}(t)\mathbf{x}(t) + \mathbf{B}_c(t)\bar{\mathbf{w}}(t) + \mathbf{E}_c\ddot{\mathbf{a}}_g(t) + \mathbf{v}(t) \tag{10}$$

where $\mathbf{x}(t)$ denotes the unobserved system state. $\mathbf{0}_n$ and $\mathbf{I}_n$ are the n^{th} order null and identity matrices respectively. $\bar{\mathbf{w}}(t)_{m\times 1}$, being the unknown ambient forcing on the structure, can be modeled as a stationary white Gaussian noise (SWGN) of constant covariance $\mathbf{Q}_{m\times m}$. $\mathbf{v}(t)$ is the process noise modeled as SWGN

with covariance $\mathbf{Q}^{v}_{2n\times 2n}$. However, no WGN model can be defined for $\ddot{\mathbf{a}}^{g}_{l\times 1}$. l is the number of channels for the disturbance input. The discrete time representation of the system is as follows,

$$\mathbf{x}_k = \mathbf{F}_k\mathbf{x}_{k-1} + \mathbf{B}_k\bar{\mathbf{w}}_k + \mathbf{E}_k\ddot{\mathbf{a}}^{g}_{k} + \mathbf{v}_k \tag{11}$$

with $\mathbf{F}_k$, $\mathbf{B}_k$, $\mathbf{E}_k$, $\mathbf{x}_k$, $\bar{\mathbf{w}}_k$, $\mathbf{x}_k$, $\mathbf{v}_k$ and $\ddot{\mathbf{a}}^{g}_{k}$ correspond to their continuous time entities described earlier, obtained through zero-order-hold technique. The system's unobserved states are estimated using dynamic strain as measurement, with the measurement equation defined as,

$$\varepsilon_k = \mathbf{H}_k\mathbf{x}_k + \mathbf{w}_k \tag{12}$$

where, $\mathbf{H}_{kp\times 2n}$ is the time dependent measurement function that maps the system states $\mathbf{x}_k$ to the corresponding strain measurements $\varepsilon_{kp\times 1}$. In reality, $\mathbf{H}_k$ signifies the strain displacement relationship modeled using the finite element approach for all the members combined. This mapping takes basis on Equation 9 and combines for all p measured members. $\mathbf{w}_{kp\times 1}$ denotes the measurement error originating from the sensor noises and can be modeled as an SWGN of constant covariance $\mathbf{R}_{p\times p}$.

3. System estimation

In the following, the system defined with the process (cf. Equation 11) and the measurement (cf. Equation 12) functions is estimated. The objective of monitoring health of the system is achieved through parameterizing the system predictor model with a set of location based health indices (HIs), which are estimated as additional time varying parameter states ξ_k from the measurement along side the contaminated system states. A typical example for HI can be a joint stiffness index, γ, that can be monitored to quantify how much damage the joint has undergone. Thus while a value of 25 denotes the joint to be perfectly healthy and rigid, a value of 0.5 (98% reduction of undamaged value) denotes the joint has become pinned type (yet not failed completely) allowing no resistance against rotation. Evidently, a high reduction in γ does not mean that severe changes in the system has happened. Thus, detection of joint damage is always more challenging than detecting a member failure.

Due to the nonlinear relationship between such health parameters with the measurements, the system estimation eventually becomes a nonlinear problem. It has to be noted this nonlinearity is only due to the time-varying parameter states, while the state propagation for regular response states is still linear. Nonlinear system estimation with Bayesian filters are typically approached with EKF, UKF, EnKF, and PF; each of them is computationally intensive. Of them, PF is appreciated as a robust approach to estimate nonlinear systems while being most compute-intensive. This article, therefore allows the parameter states to be estimated with PF while the regular response states are estimated with KF algorithm in an interacting environment. Nevertheless, the traditional KF algorithm demands the input be known exactly or at least

modeled as SWGN. With seismic or similar adverse forcing acting on the system, none of the idealizations can be proper. [54] proposed a noise robust approach with KF that employs an input rejection approach through output injection technique. In order to achieve this, the method transforms the process equation into an equation unaffected by the input noise. The same has been employed in this study, to develop a robust approach to estimate the system states and health parameters. The integration of the robust filtering approach within the IPKF environment is detailed later in this article. Prior to that, the interacting strategy has been demonstrated with the component filters (i.e. PF and KF) detailed elaborately.

3.1. Interacting filtering strategy

The interacting approach of IPKF, combining PF and KF, has already been discussed earlier in this article. Following the similar approach, PF has been employed for estimation of joint damage indices. The KF, employed as state filter is improved to induce input robustness, discussed later in this article.

For Bayesian filtering based system estimation, ideally, an explicit analytic integration is required for the entire domain of the parameters. This is however straightforward for Gaussian states with linear process and measurement equations. The current problem is nonlinear for which explicit analytical integration over the entire parameter space is not possible. Additionally, no presumption on the stochastic nature of the parameter states is enforced. PF attempts a particle approximation of this integration by propagating the system uncertainty through a cloud of N independent parameter particles $\Xi_k = [\xi^1, \xi^2, \cdots, \xi^N]$. The system dynamics is defined by the evolution of this particle set in time. At any arbitrary time step k, the evolution of an arbitrary particle ξ^j_{k-1} is a random perturbation around its current position,

$$\xi^j_k = \xi^j_{k-1} + \mathbb{N}(\delta\xi_k, \sigma^\xi_k) \tag{13}$$

where a Gaussian blurring is performed on ξ^j_{k-1} with a shift $\delta\xi_k$ and a spread of σ^ξ_k [1]. The evolved particles are subsequently weighted based on their likelihood against the current measurement.

The perturbed positions for the particles are then re-centered for consistency. This re-centring is actually a second step evolution in which particles are pushed towards the particle mean. For this, the same evolution strategy is adopted, as has been adopted in [18, 55] and is reproduced here as

$$\xi^{*j}_k = \alpha\xi^j_k + (1-\alpha)\bar{\xi}_{k-1} \tag{14}$$

where $\bar{\xi}_{k-1}$ denotes the particle mean of the parameters till time step $(k-1)$ and ξ^{*j}_k denotes the shifted position for the particle. For detailed evolution strategy, readers may refer [18]. These particles are further employed to define the system matrices $\mathbf{F}_k$, $\mathbf{B}_k$, $\mathbf{E}_k$ and the KF can then be employed to estimate the response states.

[1] $A + B\mathbb{N}(\mu, \sigma)$ means $A + Bz$ where z follows $\mathbb{N}(\mu, \sigma)$

3.2. Robust Kalman filter

Typical KF requires either the exactly known inputs or an idealized SWGN model of it. For seismic excitation, none of these idealizations is valid which calls for induction of robustness within the KF algorithm. A previously developed method [18] achieves the robustness against unknown input forces by estimating the forces in real-time through an additional force filter. This additional computation increases the overall runtime of the algorithm from the damage detection perspective. The study employs [54]'s robust approach that rejects the impact of the unknown input $\ddot{\mathbf{a}}_k^g$ in the state evolution by suitably injecting a part of the measured output in the state transition model. Owing to the measurement equation (cf. Equation 12), the following holds true for an arbitrary bounded matrix $\mathbf{G}_k \in \mathbb{R}^{2n\times m}$,

$$0 = \mathbf{G}_k \left(\varepsilon_k - \mathbf{H}_k \mathbf{x}_k - \mathbf{w}_k\right) \tag{15}$$

Adding Equation 11 with Equation 15 and further setting $\mathcal{L}_k = \mathbf{I}_{2n} - \mathbf{G}_k\mathbf{H}_k$, the state equation, Equation 11, can be modified as

$$\begin{aligned} \mathbf{x}_k &= \mathbf{F}_k \mathbf{x}_{k-1} + \mathbf{B}_k \bar{\mathbf{w}}_k + \mathbf{E}_k \ddot{\mathbf{a}}_k^g + \mathbf{v}_k + \mathbf{G}_k \left(\varepsilon_k - \mathbf{H}_k \mathbf{x}_k - \mathbf{w}_k\right) \\ &= \tilde{F}_k \mathbf{x}_{k-1} + \tilde{B}_k \bar{\mathbf{w}}_k + \tilde{E}_k \ddot{\mathbf{a}}_k^g + \mathbf{G}_k \varepsilon_k + \tilde{\mathbf{v}}_k \end{aligned} \tag{16}$$

with $\tilde{F}_k = \mathcal{L}_k\mathbf{F}_k$, $\tilde{B}_k = \mathcal{L}_k\mathbf{B}_k$, $\tilde{E}_k = \mathcal{L}_k\mathbf{E}_k$ and $\tilde{\mathbf{v}}_k = \mathbf{v}_k - \mathbf{G}_k\mathbf{w}_k$. If $\mathbf{G}_k$ is chosen such that $\mathbf{G}_k = \mathbf{E}_k(\mathbf{H}_k\mathbf{E}_k)^\dagger$, with † denoting Moore-Penrose Pseudo-inverse operation, $\tilde{E}_k$ renders to a null matrix. Equation 16 can then be transformed to Equation 17, decoupled from the unknown input $\ddot{\mathbf{a}}_k^g$ as

$$\mathbf{x}_k = \tilde{F}_k \mathbf{x}_{k-1} + \tilde{B}_k \bar{\mathbf{w}}_k + \mathbf{G}_k \varepsilon_k + \tilde{\mathbf{v}}_k \tag{17}$$

Again $\tilde{\mathbf{v}}_k$ can be idealized as an SWGN process. By this new formalism, Equation 11 has been transformed to Equation 17 in order to reject the unknown input $\ddot{\mathbf{a}}_k^g$ with an appropriate injection of the known output ε_k. Equation 12 can still be used as the associated measurement equation. With this approach, the KF can be employed without any explicit or statistical knowledge of the unknown input forces due to ground acceleration $\ddot{\mathbf{a}}_k^g$. The proof of stability and observability for this filter is given explicitly in [54].

3.3. State estimation in the nested Kalman filter

Inside the KF, state is estimated for each of the j^{th} particle. The estimation propagates current estimation ($\mathbf{x}_{k-1|k-1}^j$), conditioned on the current parameter estimate for each j^{th} particle, to the predicted value, $\mathbf{x}_{k|k-1}^j$ following Equation 18,

$$\mathbf{x}_{k|k-1}^j = \tilde{F}_k^j \mathbf{x}_{k-1|k-1}^j + \mathbf{G}_k^j \varepsilon_k \tag{18}$$

with corresponding state covariance, $\mathbf{P}^j_{k|k-1}$,

$$\mathbf{P}^j_{k|k-1} = \tilde{F}^j_k \mathbf{P}^j_{k-1|k-1} \tilde{F}^{jT}_k + \tilde{B}^j_k \mathbf{Q}_k \tilde{B}^{jT}_k + \mathbf{G}^j_k \mathbf{R}_k \mathbf{G}^{jT}_k \tag{19}$$

with $\mathbf{Q}_k$ and $\mathbf{R}_k$ being covariances of process and measurement noise.

The corresponding measurement predictions $\varepsilon^j_{k|k-1}$ can be obtained exploiting Equation 12. Associated innovation, $i^j_{k|k-1}$, can be obtained through estimating the departure of prediction from the real measurement ε_k. Next, Kalman gain, $\mathbf{K}^j_k$, is calculated as,

$$\mathbf{K}^j_k = \frac{\mathbf{P}^j_{k|k-1}\mathbf{H}^T_k}{\mathbf{S}^j_k} \tag{20}$$

where, the innovation error covariance, $\mathbf{S}^j_k = \mathbf{H}_k \mathbf{P}^j_{k|k-1} \mathbf{H}^T_k + \mathbf{R}_k$. The predicted states and state covariance are updated accordingly,

$$\mathbf{x}^j_{k|k} = \mathbf{x}^j_{k|k-1} + \mathbf{K}^j_k i^j_{k|k-1} \tag{21}$$

$$\mathbf{P}^j_{k|k} = (\mathbf{I} - \mathbf{K}^j_k \mathbf{H}_k)\mathbf{P}^j_{k|k-1} \tag{22}$$

3.4. Particle approximation

In the following, the likelihood of each particle is calculated based on the innovation mean and covariance of each KF. This likelihood information is used to update the normalized weight for each particle. The weight of j^{th} parameter particle is then estimated as

$$w(\xi^j_k) = \frac{w(\xi^j_{k-1}) P(\varepsilon_k|\xi^j_k)}{\sum_{i=1}^N w(\xi^j_{k-1}) P(\varepsilon_k|\xi^j_k)} \tag{23}$$

$P(\varepsilon_k|\xi^j_k)$ is the likelihood estimate for j^{th} particle which can be estimated as

$$P(\varepsilon_k|\xi^j_k) = \frac{1}{(2\pi)^n |\mathbf{S}^j_k|^{1/2}} e^{-\frac{1}{2}\frac{\bar{i}^{jT}_{k|k-1}\bar{i}^j_{k|k-1}}{\mathbf{s}^j_k}} \tag{24}$$

The particle approximations for the parameter and state are then estimated as

$$\begin{aligned} \mathbf{x}_{k|k} &= \sum_{j=1}^N w(\xi^j_k)\mathbf{x}^j_{k|k}; \\ \xi_k &= \sum_{j=1}^N w(\xi^j_k)\xi^j_k \end{aligned} \tag{25}$$

The proposed joint damage detection algorithm is detailed in a pseudo-code in Algorithm 1.

Algorithm 1 Proposed joint damage detection algorithm.

procedure R-IPKF($\varepsilon_k, \mathbf{Q}^v, \mathbf{R}$) ▷ Process and measurements noise covariances
  At $k = 0$ initialize particles $\{\boldsymbol{\xi}_0^j\}$ and state estimates: $\{\mathbf{x}_{0|0}^j\}$ and $\{\mathbf{P}_{0|0}^j\}$ ▷ Initialization
  for <each k^{th} measurement ε_k> **do**
    procedure R-IPKF($\{\boldsymbol{\xi}_{k-1}^j\}, \{\mathbf{x}_{k-1|k-1}^j\}, \{\mathbf{P}_{k-1|k-1}^j\}$)
      for <each particle $\boldsymbol{\xi}_k^j \in \{\boldsymbol{\xi}_k^j\}$> **do**
        evolve $\{\boldsymbol{\xi}_{k-1}^j\} \rightarrow \{\boldsymbol{\xi}_k^j\}$ ▷ Particle evolution , as per Equation (14)
        Define system matrices $\mathbf{F_k}(\boldsymbol{\xi}_k^j), \mathbf{H_k}(\boldsymbol{\xi}_k^j)$, and $\mathbf{B_k}, \mathbf{D_k}, \mathbf{E_k}$
        procedure Robust Kalman Filter ($\boldsymbol{\xi}_k^j$) ▷ For j^{th} particle
          Define $\mathbf{G_k}$, $\tilde{\mathbf{F}}_k$, $\tilde{\mathbf{B}}_k$ and $\tilde{\mathbf{v}}_k$ and realize $\bar{\mathbf{w}}_k$ from $\mathcal{N}(0, Q)$
          Predict $\mathbf{x}_{k|k-1}^j$ and $\varepsilon_{k|k-1}^j$, as per Equations (18) and (12), respectively
          Calculate innovation, $i_{k|k-1}^j$, state covariance, $\mathbf{P}_{k|k-1}^j$, and innovation error covariance, $\mathbf{S}_k^j$
          Compute Kalman gain, $\mathbf{K}_k^j$, as per Equation (20)
          Update state, $\mathbf{x}_{k|k}^j$ and state covariance, $\mathbf{P}_{k|k}^j$, as per Equations (21) and (22), respectively
        end procedure
      end for
      procedure Particle re-sampling($\{\boldsymbol{\xi}_k^j\}$)
        Calculate weight, $w(\boldsymbol{\xi}_k^j)$ for each $\boldsymbol{\xi}_k^j \in \{\boldsymbol{\xi}_k^j\}$ and re-sample ▷ see Equation (23)
        Calculate, $\mathbf{x}_{k|k}$ and parameter estimate, $\bar{\boldsymbol{\xi}}_k$ ▷ see Equation (25)
      end procedure
    end procedure
  end for
end procedure

4. Numerical experiment

The proposed algorithm has been numerically validated on a three story - three bay, 2-dimensional (2-D) steel shear frame. The bay width is $4m$ while the height of each column is $3m$. The frame is made up of 21 members (12 columns and 9 beams) and 12 joints, where all the members are assumed to have the properties of the Indian Standard Wide Flange Beam, ISWB450 [59] (cf. Table 1). Figure 2 demonstrates the schematic diagram of the frame with its member and node numbers. Each node has 3 *dof*s. A 6-*dof* Euler-Bernoulli beam element has been employed for the numerical modeling of the frame.

Table 1: Properties of ISWB450.

Weight per metre (kg/m)	**Section area** (cm^2)	**Depth of section** (mm)	**Width of flange** (mm)	**Moment of inertia**, I_{xx} (cm^4)	**Moment of inertia**, I_{yy} (cm^4)
79.40	101.15	450	200	35057.60	1706.70

The defined frame is subjected to an earthquake excitation along with an additional ambient forcing, modeled as an SWGN, applied for the entire simulation time. North-South component of the El-Centro earthquake ground motion data (May 18, 1940 in CA, USA) (Data source: `http://peer.berkeley.edu/research/motions/`) has been employed as the earthquake base excitation. Rayleigh's viscous damping model has been employed for the simulation. For all the numerical case studies, the seismic force is applied one second after the start of the simulation, followed by a damage induced in the joint/s two seconds later

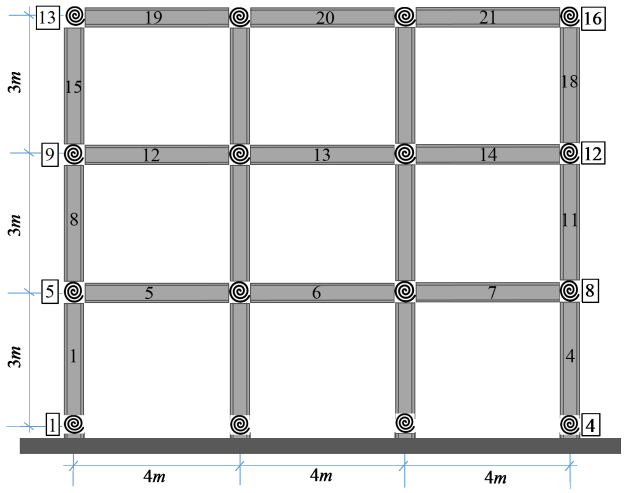

Figure 2: 2-D three bay three story steel shear frame.

(unless specified otherwise for some cases), for the sake of practicality. Damage in the joint/s are induced in the numerical model through fractional reduction of their corresponding undamaged joint stiffness indices. For better understanding, all the joints are initially considered as rigid/perfectly fixed with their joint stiffness indices, $\gamma_0 = 25$. The algorithm then estimates the deterioration in this index values to localize and quantify damage in the joints. It should be noted that the capacity of the algorithm is not limited to rigid frames only and can be employed for semi-rigid frames having initial γ_0 less than 25.

The responses from strain gauges are sampled at a fixed sampling frequency of 50 Hz for 20.48s to collect 1024 long time series of dynamic strain. In general, an SWGN of 2% signal-to-noise ratio (SNR)[2] is added to the measured response obtained only from the columns {1:4 8:11 15:18} for most of the cases, unless stated otherwise. The strain gauges are patched on the outer surface of the columns and bottom surface of the beams, at their mid span. Initial distribution type for the parameter particles is set to be Gaussian with their undamaged joint stiffness index values (i.e., 25) set as particle mean with standard deviation of 0.25. The assumed value for α is 0.98 (cf. Equation 14). The evolution of the parameter particles are entirely dictated by the PF based on their relative likelihoods against measurements. It can be presumed without much contradiction that a higher number of particles typically yields a better precision in the estimate, which however increases the computational cost. To start with, a set of 3000 particles has been observed to be sufficient for the parameter estimation which also corroborates the authors' earlier experiences with typical applications of IPKF on other problems.

4.1. Frequency response of the system

The frame is subjected to an SWGN forcing of unit variance, $\mathbb{N}(0, 1)$ N^2, on all its nodal *dof*s, from the beginning of the simulation. As detailed earlier, the earthquake force is applied as base excitation along

[2]In this study, an x% SNR SWGN signifies the ratio of standard deviation of SWGN noise to signal being 2%

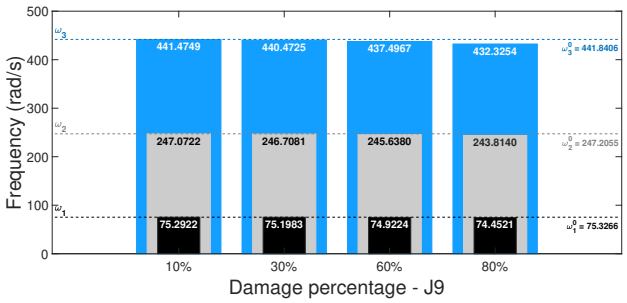

Figure 3: Frequency response of the undamaged and damaged frame.

the horizontal direction (as per the Figure 2) of the frame after the first second of the simulation. The same system is further tested with induced damage in its ninth joint (J9) of severities 10%/30%/60%/80% (corresponding to $\gamma = 22.5/17.5/10/5$). The recorded responses have been put through a modal domain decomposition to have an idea of the induced change in the first three natural frequencies. It has been observed that the change in the first three natural frequencies (here, ω_1, ω_2 and ω_3) due to the induced damage is low even for an 80% damage in the joint (maximum of 2.15% for ω_3 compared to 10.71% change for the same damage severity in the 10^{th} member of the frame) (cf. Figure 3). This negligible difference hence establishes the fact that the impact of joint damage on the global dynamical properties of the structures is mostly very weak and one needs a strong detection algorithm in order to trace out any changes caused by the joint damage. For joint damage detection in real life structures, these minuscule changes due to damage gets further masked, therefore become imperceptible, especially when the structure, the recorders and the predictor model are susceptible to ambient vibration, measurement noise, and model uncertainties, respectively. This clearly justifies the application of a time domain probabilistic approach capable of dealing with the associated uncertainties while performing accurately in detection.

4.2. Comparison between r-IPKF and IPKF

Prior to investigating the accuracy of the proposed method for joint damage detection, the inclusion of robustness against input noise is justified. The overall advantage of the robust IPKF (r-IPKF) over IPKF is demonstrated in this section. The performance of both algorithms is studied for three cases (cf. Figure 4): 1) linear time variant (LTV) system subjected only to SWGN forcing; 2) linear time invariant (LTI) system subjected to SWGN and earthquake (EQ); and 3) LTV system subjected to SWGN and EQ. For the sake of clarity in understanding, the estimation of joint stiffness index, γ_{dam}, of the damaged joint (J9) is presented along with the joint stiffness index, γ_{undam}, of one of the undamaged joints (J5) in all the figures from here on.

It is evident from the Figure 4, that both algorithms perform equally well when an LTV system is subjected to an SWGN input (cf. Figure 4a), thereby suggesting that a temporal variation in the system does not affect their efficacy. In the absence of damage (cf. Figure 4b), the non-robustness against input

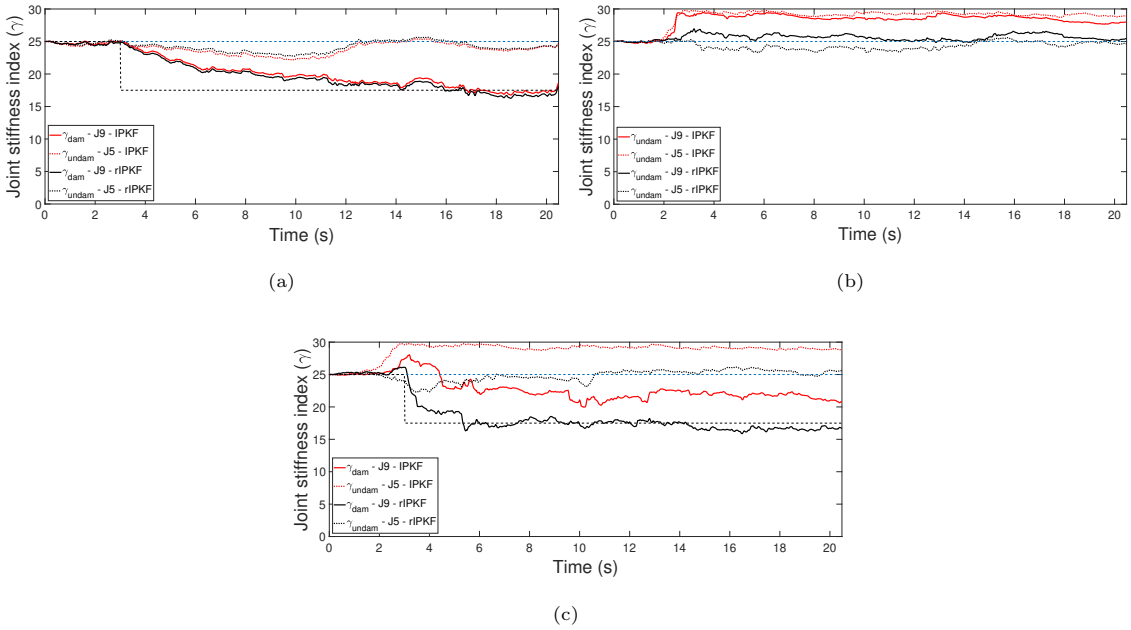

Figure 4: Comparative study between r-IPKF vs. IPKF for various systems and inputs: (a) LTV system with SWGN input; (b) LTI system with SWGN and EQ inputs; and (c) LTV system with SWGN and EQ inputs.

statistics variation in IPKF is observed to affect the estimation severely when the system is subjected to a non-stationary forcing (here earthquake excitation). Eventually, the algorithm converged to a wrong set of estimates for the joint stiffness indices. This test case establishes that the divergence in the estimation can happen with IPKF due to non-stationary forces alone, even in the absence of damage. For case 3), r-IPKF accurately and precisely localizes the damage and is observed to be very stable (cf. Figure 4c). The induced robustness in the state filter of r-IPKF perfectly removed the variations arising from the input as if the input never existed. Further, for a system with damage (30% of γ_0) as well as with non-stationary forcing, Figure 4c depicts how r-IPKF outperforms the IPKF algorithm. This numerical study presents that an accurate estimation can never be achieved with the standard IPKF algorithm, unless the forcing model is stationary and/or exactly known. r-IPKF, on the other hand, does not demand such information and therefore provides more reliable and stable estimates.

4.3. Estimation accuracy with the proposed r-IPKF approach

In the following, the estimation accuracy of the proposed method is investigated. The algorithm is found to estimate the state variables, i.e., displacements and velocities, within a close proximity to their true values obtained from the numerical simulation. Figure 5 shows a comparison between the estimated (mean) and the true (uncontaminated) displacement time series for the 13^{th} *dof*, i.e., *x-direction* for J9. The simulation specification of the employed forcing (SWGN and EQ), is the same as in Section 4.1 with a 30% damage induced 3 seconds after the start of the simulation. The error in estimation is observed to shoot up (cf.

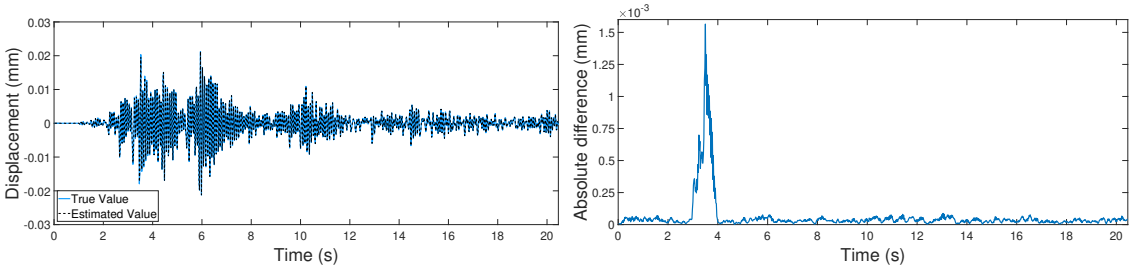

(a) (b)

Figure 5: Comparison between estimated state (mean) and true displacement values: (a) Estimated state (mean) vs. true displacement values; and (b) Absolute difference between estimated state(mean) and true displacement values.

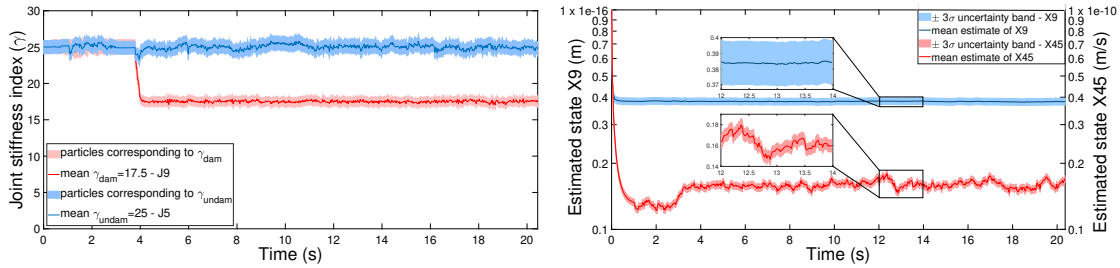

(a) (b)

Figure 6: Evolution of parameters and states: (a) Particle evolution in time for damaged and undamaged joints; and (b) Estimated state with $\pm 3\sigma$ uncertainty bounds (*X9 and X45 are the* 9^{th} *and* 45^{th} *component of state vector. The* $\pm 3\sigma$ *uncertainty bands denote the* $\pm 3\sigma$ *limits of the Gaussian uncertainty*).

Figure 5b) on introduction of damage in the system, which, however, is brought back to an acceptable limit through prompt and efficient estimation of the joint damage parameters. The estimation error is observed to be almost consistent throughout, not affected by the intensity of the input forcing. This ensures the much required stability in the algorithm even in the case of sudden introduction of changes in terms of forcing or system model. The corresponding particle evolution of the health parameters, γ_{dam} (J9) and γ_{undam} (J5), over time is presented in Figure 6a. The state estimates and their covariances have also been observed to be stable and not exploding over prolonged estimation (cf. Figure 6b).

4.4. Detection of various damage extents

With a 2% SNR contaminated measurement signal, the extent of damage level that can be detected with the proposed r-IPKF has been tested against several damage severities. Four different damage levels are selected: 10%/30%/50% and 70% with corresponding γ value as: 22.5/17.5/12.5 and 7.5 (cf. Figure 7). For the sake of unbiased comparison, the damage is induced consistently at J9, while the estimation is performed using strain measurements collected from all the columns, for all the case studies. Figure 7 demonstrates that the algorithm is efficient in detecting and localizing weak damage as small as 10% ($\gamma = 22.5$). However, it can also be perceived from the figure that for small damage cases, the estimation may at times get masked due to the sensor noises. Keeping this aspect into consideration, a minimum of 20% joint damage can

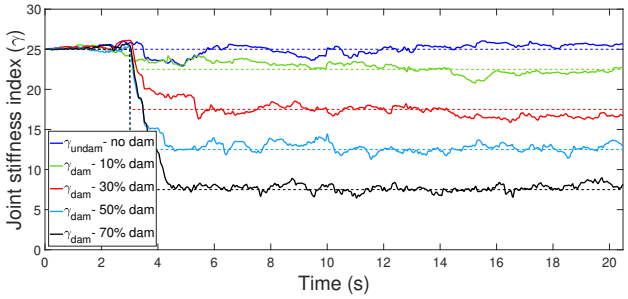

Figure 7: Extent of damage level detected by r-IPKF algorithm.

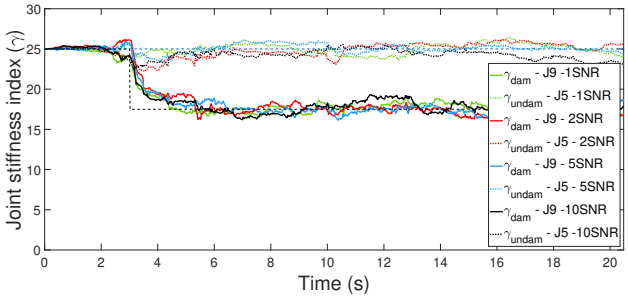

Figure 8: Measurement noise sensitivity of r-IPKF algorithm

certainly be detected without any confusion.

4.5. Measurement noise sensitivity

To check the sensitivity of the proposed r-IPKF algorithm to increasing noise levels, a set of numerical case studies has been taken up. For this, an uncontaminated dataset of dynamic strain time histories (numerically simulated) has been first contaminated with increasing noise levels of SNR value 1/2/5/10 % and further employed for detection of joint damage with the proposed r-IPKF algorithm. The results are presented in Figure 8. It has been observed that even with a noise level of 10% SNR, the algorithm remained prompt and precise in detection, for all the cases. No undamaged joints are falsely detected for any of the above mentioned noise levels.

4.6. Effect of number, location and vicinity of strain gauges

The unique advantage of the proposed r-IPKF based algorithm, which uses strain gauges over accelerometers, is that the approach is much cheaper by using this type of sensor. Strain gauges are typically much less costly than accelerometers and are also frame invariant, i.e., they yield consistent response even in the presence of base excitation. In contrast, the accelerometers can not provide the relative accelerations of the structure in case of base excitation. Furthermore, strain measurement has been reported to be more sensitive to damage in several studies.

The impact of different numbers and locations for the employed strain gauges on the estimation accuracy has further been investigated in this study. When monitoring the health of a real life structure, damage

Table 2: Sensor number and location sensitivity.

C.No.	No. of sensors	Sensor location	Detection - J9	Accuracy (%)	False positives
1	21	All members {1:21}	✓	99.02	×
2	12	Only columns {1:4 8:11 15:18}	✓	97.77	×
3	9	Only beams {5:7 12:14 19:21}	×	-	-
4	6	Only external columns {1 4 8 11 15 18}	✓	95.31	✓
5	6	Only external beams {5 7 12 14 19 21}	×	-	-

identification depends on the observability of the system states with respect to the considered state space model and the sensitivity of the parameters with respect to the measurements. Hence, the effect of sensor number on the damage identification results does not justify the efficacy of the algorithm. However a methodological investigation on the effect of number and location of sensors has been undertaken in this study, the results of which should nevertheless be considered specific to the current problem and model. Five test cases are investigated with: 1) strain gauges patched on all the members; 2) strain gauges patched only on the columns; 3) strain gauges patched only on the beams; 4) strain gauges patched on the external columns; and 5) strain gauges patched on the external beams. The results are presented in the Table 2. For the sake of comparison, simulation specifications like damage location, extent and noise levels are kept the same as in Section 4.3.

It is observed that damage is detected promptly and accurately as long as the responses of the columns are employed for the estimation. The responses only from beams, failed to yield a reliable estimation even for low (1%) noise contamination levels. This indicates the possibility that the joint damage leaves very weak signature in the beam responses under the mentioned forcing. It has further been confirmed from the simulation results that the beam responses are remarkably weaker than that of the columns which can be attributed to the poor performance of the proposed algorithm with beam responses only. It has also been observed that the estimation is prone to deteriorate with the decrease in sensor number and may cause infrequent false alarms.

A separate study has also been undertaken to check the effect of placement of the sensors in the vicinity of the damaged joint (J10). Three sets of members are selected for measurement for this study, named as: near, far, and farthest. The classification and nomenclature of the sets take basis on their distances from the damaged joint. For the near case, members attached to the damaged joint have been measured and subsequently, the measured response has been employed for detection. An accuracy of 87.88%, when compared to an expected γ value of 17.5 (= 30% damage), has been achieved with such measurement (cf. Figure 9). Nevertheless, measurements obtained from far members when employed for estimation, give an improved accuracy of 93.93%. The improvement is due to selection of four columns' strain response for measurement. The better sensitivity of the column responses to joint damage over the beam responses has

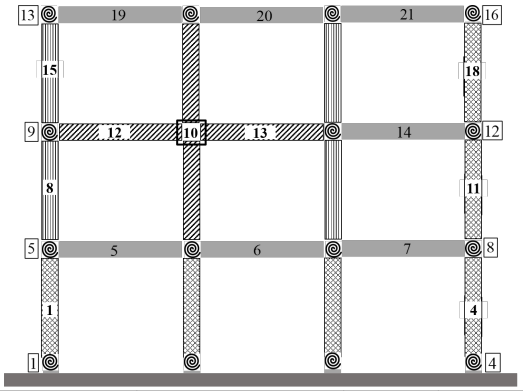

Damage location	Sensor vicinity	Detection	Accuracy
J10 - 30% dam	Near **{9 12 13 16}**	✓	87.88%
	Far **{8 10 15 17}**	✓	93.93%
	Farthest **{1 2 3 4 11 18}**	×	-

Figure 9: Effect of sensors placed at varying vicinity from the damaged joint.

already been discussed in this article, which further gets manifested with this numerical case study. Finally, with measurements from the farthest members, very poor estimation has been observed which indicates that the impact of joint damage for this particular structural arrangement gets attenuated for members far away from the damage location.

Further, it must be emphasized that the detection ability of any SHM algorithm depends on several factors, such as sensor density, measurement type and quality, sensor location and vicinity, etc. The perfect combination of all these attributes that results in an optimal approach is very much case specific. Like in the case study demonstrated, it has been found that column responses are better damage sensitive than beam responses. Also, when algorithm performance has been compared based on sensor vicinity, it has been found that nearby sensors are more likely to detect a damage. However, there has been an observation that column responses collected from far locations (4 nos) provide better damage sensitive response compared to nearby beam and column responses (2 no beam and 2 no column). This clearly establishes the fact that signal quality plays a bigger role than sensor vicinity for this particular structure. Finally, it should be mentioned here that this experience is very much case specific. A change in the structural configuration can all together provide a completely different experience.

4.7. Stability Check

The algorithm is further checked for its stability, the possibility of divergence, and error accumulation in case of prolonged usage. For this, a time series of 307.2s has been tested with the proposed algorithm. The dataset corresponds to a structure similar to what has been described in Section 4.3, only the time of simulation has been extended to 307.2s involving 15360 data points in time. The algorithm performed well throughout the entire simulation showing no sign of instability or divergence at any stage of the estimation (cf. Figure 10).

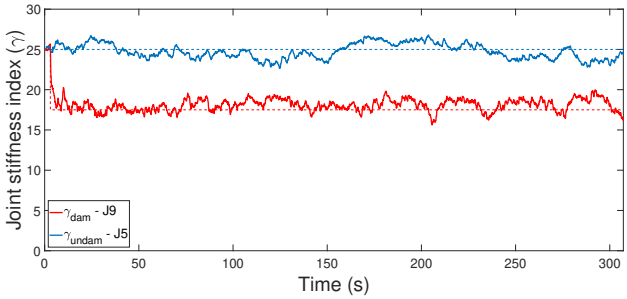

Figure 10: Stability check of the algorithm.

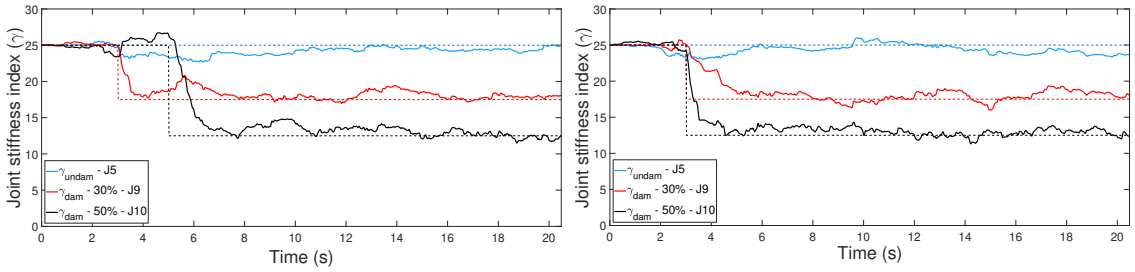

(a) (b)

Figure 11: Joint damage estimation for multiple damage scenarios: (a) Non-simultaneous multiple damage; and (b) Simultaneous multiple damage.

4.8. Detection of multiple damage

The proposed algorithm is further examined for its robustness towards multiple damage situation involving varying damage levels as well as simultaneity/non-simultaneity of these damage occurrences (cf. Figure 11). The following two cases have been studied: 1) 30% damage in J9 followed by 50% damage in J10 - 3s and 5s after the start of simulation, respectively (cf. Figure 11a); and 2) simultaneous 30% damage ($\gamma = 17.5$) in J9 and 50% damage ($\gamma = 12.5$) in J10 - 3s from the start of simulation (cf. Figure 11b).

A 2% SNR has been used to contaminate the strain data. Damage locations, severities as well as simultaneity are identified with a sufficient level of promptness and accuracy for both of the above cases (cf. Figure 11).

An additional investigation has been performed to see how the joint damage detection algorithm behaves in the presence of member damage (and no actual joint damage). In this case, the member has been damaged in place of the joints and the response has been analysed with the proposed algorithm which is built with an assumption on joint damage. A 60% reduction in the initial elasticity (assumed as member damage) for the 10^{th} member (cf. Figure 12) is induced in the simulator model. Keeping other simulation specifications same as before, the strain measurements are collected from all the columns prior to contaminating them with measurement noise of 2% SNR SWGN. With the proposed algorithm, the joints attached to the 10^{th} member have been identified as damaged with damage value roughly around 70% in J11 (upper joint) and 50% in J7 (lower joint). The simultaneity in detection for damage in two joints may faintly indicate the

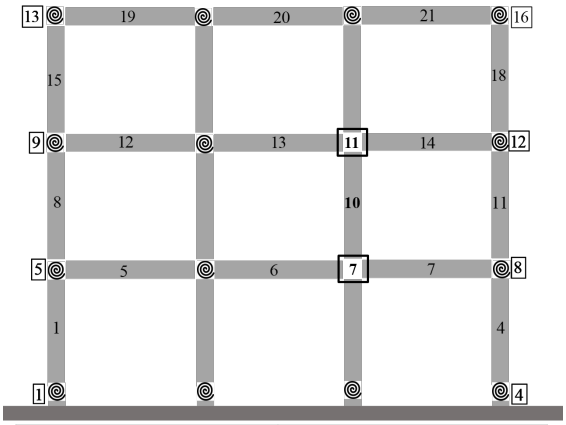

Damage induced member	Damage detected in joints
10 – 60% damage	**J11** – 70% damage
	J7 – 50% damage

Figure 12: Performance of algorithm to identify member damage.

possibility of damage in the attached member, instead of the joints. From this experiment, it is obvious that even though the algorithm is not equipped with member damage detection capability, one can still isolate the damaged member effectively, just from the location of the damaged joints.

5. Experimental Validation

The proposed algorithm is experimentally validated on a 2-D steel frame, cf. Figure 13. The center-to-center lengths of the beams are 408 mm whereas the column heights are taken as 333.3 mm uniformly. The cross-sectional areas for all the beams and columns are 6 $mm \times 6$ mm and 8 $mm \times 8$ mm, respectively. Accordingly, a supporting numerical frame model using the methodology demonstrated earlier is prepared. The joints are 3-D printed with high density polyethylene (HDPE) with a thickness of 3 mm encapsulating the beam and column ends. To ensure a monolithic rigid joint, both ends of the beams are rested on top of the column ends with no gap in between. A primary calibration of the material properties has been attempted to match the frequencies obtained from experimental structure to that of the numerical support structure, details of which will be elaborated in the following. The geometric and calibrated material properties of the frame are stated in Table 3.

5.1. Calibration of numerical model

Three strain gauges, placed on each of the three beams, have been employed for the study. The dynamic response is sampled at fixed sampling frequency of 1000 Hz. Subsequently, the measured strain response is decomposed in frequency domain using the frequency domain decomposition (FDD) approach. The frequency response function (FRF) showcasing the first two frequencies, $\omega_1 = 9.033\ Hz$, and $\omega_1 = 36.377\ Hz$,

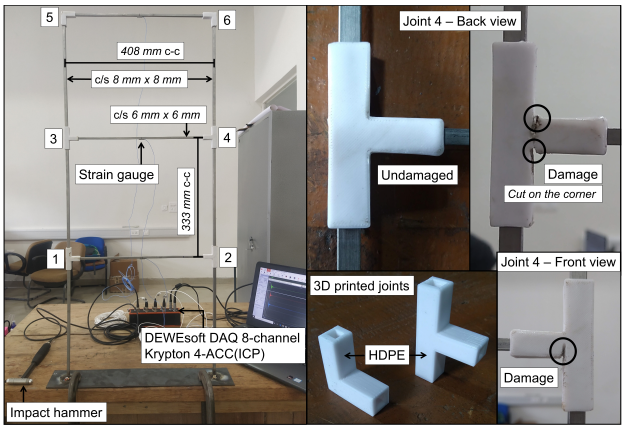

Figure 13: Experimental setup with damage specification in J4 - 2-D frame.

Table 3: Properties of 2-D steel frame.

Length of beam	400 mm
Cross-section area of beams	6 $mm \times 6$ mm
Frame height	1000 mm
Cross-section area of columns	8 $mm \times 8$ mm
Calibrated modulus of elasticity	150 GPa
Calibrated density	8000 Kg/m^3
Damping ratio	0.02

obtained from FDD of the experimental strain data can be found in Figure 14a. Material characteristics, i.e., modulus of elasticity E and density ρ, of the numerical frame model are further updated (cf. Table 3) to approximately match the modal properties of the experimental structure (cf. Figure 14b). The calibrated model can thus be assumed to replicate the experimental frame dynamics with sufficient accuracy.

For further fine tuning the numerical model to replicate the real structure, γ values are calibrated which also helped to provide with the undamaged stiffness index of the joints. Transient response of 0.5 s (500 data points) has been used with the proposed r-IPKF approach to estimate the six γ indices corresponding

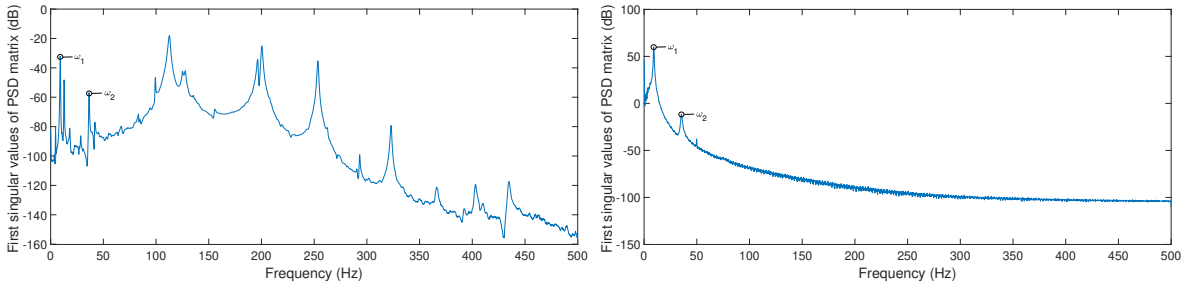

(a) (b)

Figure 14: Calibration of the 2-D frame by comparing frequencies obtained from Frequency Domain Decomposition (FDD), ω_1, and ω_2 *are the first, and second frequency of the structure, respectively*:
(a) FDD of strain data obtained from the experiment ($\omega_1 = 9.033$ Hz, and $\omega_1 = 36.377$ Hz); and
(b) FDD of strain data obtained from calibrated numerical model($\omega_1 = 9.033$ Hz, and $\omega_2 = 35.400$ Hz).

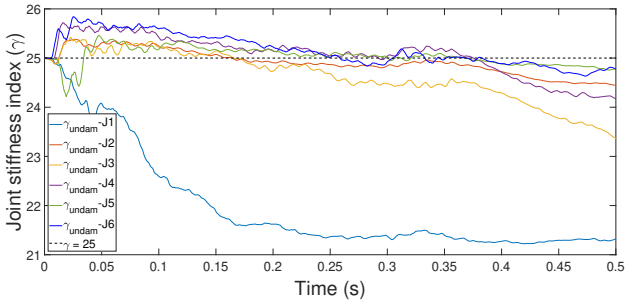

Figure 15: Bench marking γ with respect to undamaged 2-D frame.

to each of the joints (J1-J6). The algorithm is employed with 3000 particles and $\alpha = 0.98$ (cf. Equation 14) with an initial stiffness estimate for the joints as 25 (i.e., perfectly healthy and rigid joint condition). The algorithm further estimated the γ values under the initial undamaged condition (cf. Figure 15). While most of the joints are observed to keep maintaining its initial position, a few drifted away denoting the conjecture on its rigidity was not proper.

5.2. Experimental verification of the proposed approach

The outcome of the last estimation process yielded a better model for the real structure to be used for the predictor model with the updated values for the joint stiffness γ replicating the current health of the undamaged structure. Next, a damage is inflicted in J4, cf. Figure 13, by cutting the HDPE joint up to the beam-column interface on three corners. The transient response of the damaged frame is further sampled at 1000 Hz for one second and employed as the measurement in the proposed algorithm. It can be verified from the Figure 16a, that the proposed algorithm is capable of identifying, localizing and quantifying damage in the joint. The estimation of damage in J4 has been compared against J6. A significant reduction in γ corresponding to J4 ($\gamma = 10$) from its original value (i.e. $\gamma = 24$) can easily be isolated and quantified. The estimation has been observed to be stable and convergent for both damaged and healthy joints.

It has further been observed that a minimum of two sensors, placed in the middle at the bottom-side of the lower and the middle beam (connected to damaged joint) is required for joint damage detection. Since maximum stress occurs at the surface of the beam farthest from the neutral axis and generally the bottom-side of the beam is accessible, hence strain sensors have been patched to the bottom-side of the beam. The algorithm promptly detected the damage and depicted a similar detection accuracy, c.f. Figure 16b as compared to that obtained from the previous sensor placement (c.f. Figure 16a).

It has to be noted that, insufficient instrumentation for the structure may hamper the observability conditions for high dimensional systems. This requirement of measurement sufficiency renders the scalability issue for the proposed algorithm to be a relative aspect that should consider the system size (n_s) and the number of available measurement channels (n_m). This allows the scalability issue to be discussed in the light of reducing available measurement channels instead of increasing system size, which has been attempted

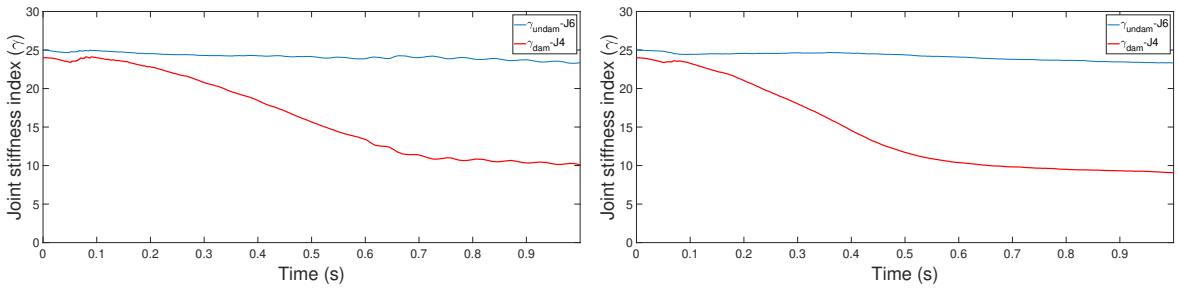

Figure 16: Joint damage detection of 2-D frame by the proposed approach,
(a) placing one sensor on each beam (3 sensors); and (b) placing only 2 sensors.

with the real frame model.

Denoting this ratio between n_s and n_m as Δ, it has been observed that the current study has maintained a very high value for this index (9 for both numerical and experimental studies), i.e., relatively high dimensional structures can be monitored with limited sensors. The same when put to comparison with existing literature dealing with real scale models can be observed not to be significantly different.

6. Conclusion

This paper deals with joint damage detection and localization in a semi-rigid frame structure which is mostly ignored in the traditional SHM studies. The robust Interacting Particle-Kalman filtering (r-IPKF) approach is employed to simultaneously estimate response states while estimating the joint health through a set of health parameters. Further, to enhance its practical usage, strain responses have been adopted as the measurement because of their low cost and frame invariability in the case of base excitation conditions compared to accelerometers. The predictor model involved, however, requires an efficient mapping for nodal displacements to strain measurements, specific to semi-rigid frames. This study, therefore, derives the strain-displacement relationship for the semi-rigid frames. To induce robustness in the detection against arbitrary input forcing, the state filter within IPKF is improvised through an output injection technique that renders the algorithm robust to any forcing types. The algorithm is tested for its efficacy against non-stationary forcing, measurement noise, damage levels, and stability criteria on a 2-D semi-rigid frame structure. It has been found that the algorithm can detect damage in joints for most of the mentioned conditions with sufficient promptness and accuracy. It has also been demonstrated that with the present algorithm, a possibility of member damage can also be detected, although not supported with in depth investigation for the sake of brevity. The proposed algorithm is experimentally tested on a 2-D steel frame and is observed to be efficient and accurate in detecting joint damage.

Acknowledgements

The authors gratefully acknowledge the support of this research by Science & Engineering Research Board (SERB), New Delhi, India, through grant file no. ECR/2018/001464.

References

[1] Hasan N Katkhuda, Hazim M Dwairi, and Nasim Shatarat. System identification of steel framed structures with semi-rigid connections. *Structural engineering & mechanics*, 34(3):351, 2010.

[2] Ying Lei, Qing Li, Feng Chen, and Zhiwei Chen. Damage identification of frame structures with joint damage under earthquake excitation. *Advances in Structural Engineering*, 17(8):1075–1087, 2014.

[3] OS Salawu. Detection of structural damage through changes in frequency: a review. *Engineering structures*, 19(9):718–723, 1997.

[4] Scott W Doebling, Charles R Farrar, Michael B Prime, et al. A summary review of vibration-based damage identification methods. *Shock and vibration digest*, 30(2):91–105, 1998.

[5] Scott W Doebling, Charles R Farrar, Michael B Prime, and Daniel W Shevitz. Damage identification and health monitoring of structural and mechanical systems from changes in their vibration characteristics: a literature review. Technical report, Los Alamos National Lab., NM (United States), 1996.

[6] Ying Lei, Feng Chen, and Huan Zhou. An algorithm based on two-step kalman filter for intelligent structural damage detection. *Structural Control and Health Monitoring*, 22(4):694–706, 2015.

[7] Chung-Bang Yun, Jin-Hak Yi, and Eun Young Bahng. Joint damage assessment of framed structures using a neural networks technique. *Engineering structures*, 23(5):425–435, 2001.

[8] Jian-Huang Weng, Chin-Hsiung Loh, and Jann N Yang. Experimental study of damage detection by data-driven subspace identification and finite-element model updating. *Journal of structural engineering*, 135(12):1533–1544, 2009.

[9] WD Zhu and K He. Detection of damage in space frame structures with l-shaped beams and bolted joints using changes in natural frequencies. *Journal of Vibration and Acoustics*, 135(5):051001, 2013.

[10] Sopon Ritdumrongkul, Masato Abe, Yozo Fujino, and Takeshi Miyashita. Quantitative health monitoring of bolted joints using a piezoceramic actuator–sensor. *Smart materials and structures*, 13(1):20, 2003.

[11] Derek Doyle, Andrei Zagrai, Brandon Arritt, and Hakan Çakan. Damage detection in bolted space structures. *Journal of Intelligent Material Systems and Structures*, 21(3):251–264, 2010.

[12] Colin Haynes, Michael Todd, Takeaki Nadabe, and Nobuo Takeda. Monitoring of bearing failure in composite bolted connections using ultrasonic guided waves: A parametric study. *Structural Health Monitoring*, 13(1):94–105, 2014.

[13] Zilong Wang and Young-Jin Cha. Unsupervised deep learning approach using a deep auto-encoder with an one-class support vector machine to detect structural damage. *Structural Health Monitoring*, page 1475921720934051, 2020.

[14] Young-Jin Cha and Zilong Wang. Unsupervised novelty detection–based structural damage localization using a density peaks-based fast clustering algorithm. *Structural Health Monitoring*, 17(2):313–324, 2018.

[15] Guillaume Mercère, Laurent Bako, and Stéphane Lecœuche. Propagator-based methods for recursive subspace model identification. *Signal Processing*, 88(3):468–491, 2008.

[16] Ivan Goethals, Laurent Mevel, Albert Benveniste, and Bart De Moor. Recursive output-only subspace identification for in-flight flutter monitoring. In *Proceedings of the 22nd International Modal Analysis Conference (IMACXXII), Dearborn, Michigan*, 2004.

[17] Guillaume Mercère, Stéphane Lecoeuche, and Marco Lovera. Recursive subspace identification based on instrumental variable unconstrained quadratic optimization. *International Journal of Adaptive Control and Signal Processing*, 18(9-10):771–797, 2004.

[18] Subhamoy Sen, Antoine Crinière, Laurent Mevel, Frédéric Cérou, and Jean Dumoulin. Seismic-induced damage detection through parallel force and parameter estimation using an improved interacting particle-kalman filter. *Mechanical Systems and Signal Processing*, 110:231–247, 2018.

[19] Subhamoy Sen and Baidurya Bhattacharya. Online structural damage identification technique using constrained dual extended kalman filter. *Structural Control and Health Monitoring*, 24(9):e1961, 2017.

[20] Hasan Katkhuda, Nasim Shatarat, and Khaled Hyari. Damage detection in steel structures with semi-rigid connections using unscented kalman filter. *International Journal of Structural Integrity*, 2017.

[21] Costas Papadimitriou, Claus-Peter Fritzen, Peter Kraemer, and Evangelos Ntotsios. Fatigue predictions in entire body of metallic structures from a limited number of vibration sensors using kalman filtering. *Structural Control and Health Monitoring*, 18(5):554–573, 2011.

[22] Jianye Ching, James L Beck, and Keith A Porter. Bayesian state and parameter estimation of uncertain dynamical systems. *Probabilistic engineering mechanics*, 21(1):81–96, 2006.

[23] Alberto Corigliano and Stefano Mariani. Parameter identification in explicit structural dynamics: performance of the extended kalman filter. *Computer Methods in Applied Mechanics and Engineering*, 193(36-38):3807–3835, 2004.

[24] Alberto Corigliano, Martino Dossi, and Stefano Mariani. Model order reduction and domain decomposition strategies for the solution of the dynamic elastic–plastic structural problem. *Computer Methods in Applied Mechanics and Engineering*, 290:127–155, 2015.

[25] Lennart Ljung. Asymptotic behavior of the extended kalman filter as a parameter estimator for linear systems. *IEEE Transactions on Automatic Control*, 24(1):36–50, 1979.

[26] Arnaud Doucet, Nando De Freitas, Kevin Murphy, and Stuart Russell. Rao-blackwellised particle filtering for dynamic bayesian networks. In *Proceedings of the Sixteenth conference on Uncertainty in artificial intelligence*, pages 176–183. Morgan Kaufmann Publishers Inc., 2000.
[27] Pierre Del Moral and Feynman-Kac Formulae. Genealogical and interacting particle systems with applications. probability and its applications, 2004.
[28] Subhamoy Sen and Baidurya Bhattacharya. Progressive damage identification using dual extended kalman filter. *Acta Mechanica*, 227(8):2099–2109, 2016.
[29] Saeed Eftekhar Azam, Aldo Ghisi, and Stefano Mariani. Parallelized sigma-point kalman filtering for structural dynamics. *Computers & Structures*, 92:193–205, 2012.
[30] Zhe Chen et al. Bayesian filtering: From kalman filters to particle filters, and beyond. *Statistics*, 182(1):1–69, 2003.
[31] Masaru Hoshiya and Etsuro Saito. Structural identification by extended kalman filter. *Journal of engineering mechanics*, 110(12):1757–1770, 1984.
[32] Simon J Julier and Jeffrey K Uhlmann. New extension of the kalman filter to nonlinear systems. In *Signal processing, sensor fusion, and target recognition VI*, pages 182–194. International Society for Optics and Photonics, 1997.
[33] Stefano Mariani and Aldo Ghisi. Unscented kalman filtering for nonlinear structural dynamics. *Nonlinear Dynamics*, 49(1-2):131–150, 2007.
[34] B Radhika and CS Manohar. Nonlinear dynamic state estimation in instrumented structures with conditionally linear gaussian substructures. *Probabilistic Engineering Mechanics*, 30:89–103, 2012.
[35] B Radhika and CS Manohar. Updating response sensitivity models of nonlinear vibrating structures using particle filters. *Computers & Structures*, 89(11-12):901–911, 2011.
[36] Eleni N Chatzi and Andrew W Smyth. The unscented kalman filter and particle filter methods for nonlinear structural system identification with non-collocated heterogeneous sensing. *Structural Control and Health Monitoring: The Official Journal of the International Association for Structural Control and Monitoring and of the European Association for the Control of Structures*, 16(1):99–123, 2009.
[37] S Eftekhar Azam, M Bagherinia, and Stefano Mariani. Stochastic system identification via particle and sigma-point kalman filtering. *Scientia Iranica*, 19(4):982–991, 2012.
[38] Chris Snyder, Thomas Bengtsson, Peter Bickel, and Jeff Anderson. Obstacles to high-dimensional particle filtering. *Monthly Weather Review*, 136(12):4629–4640, 2008.
[39] Milad Roohi, Kalil Erazo, David Rosowsky, and Eric M Hernandez. An extended model-based observer for state estimation in nonlinear hysteretic structural systems. *Mechanical Systems and Signal Processing*, 146:107015, 2021.
[40] Milad Roohi, Eric M Hernandez, and David Rosowsky. Reconstructing element-by-element dissipated hysteretic energy in instrumented buildings: application to the van nuys hotel testbed. *Journal of Engineering Mechanics*, 147(1):04020141, 2021.
[41] Rickard Karlsson, Thomas Schon, and Fredrik Gustafsson. Complexity analysis of the marginalized particle filter. *IEEE Transactions on Signal Processing*, 53(11):4408–4411, 2005.
[42] Meriem Zghal, Laurent Mevel, and Pierre Del Moral. Modal parameter estimation using interacting kalman filter. *Mechanical Systems and Signal Processing*, 47(1-2):139–150, 2014.
[43] Antoine Crinière, Meriem Zghal, Laurent Mevel, and Jean Dumoulin. Gpgpu implementation of modal parameter tracking by particle based kalman filter. In *8th European Workshop On Structural Health Monitoring (EWSHM 2016)*, 2016.
[44] Subhamoy Sen, Antoine Crinière, Laurent Mevel, Frédéric Cérou, and Jean Dumoulin. Estimation of time varying system parameters from ambient response using improved particle-kalman filter with correlated noise. In *EGU General Assembly Conference Abstracts*, page 15527, 2017.
[45] Yang Li, Yaozhi Luo, Hua-Ping Wan, Chung-Bang Yun, and Yanbin Shen. Identification of earthquake ground motion based on limited acceleration measurements of structure using kalman filtering technique. *Structural Control and Health Monitoring*, 27(1):e2464, 2020.
[46] Ai-Lun Wu, Chin-Hsiung Loh, Jann N Yang, Jian-Huang Weng, Chia-Han Chen, and Tzou-Shin Ueng. Input force identification: application to soil–pile interaction. *Structural Control and Health Monitoring: The Official Journal of the International Association for Structural Control and Monitoring and of the European Association for the Control of Structures*, 16(2):223–240, 2009.
[47] Ying Lei, Dandan Xia, Kalil Erazo, and Satish Nagarajaiah. A novel unscented kalman filter for recursive state-input-system identification of nonlinear systems. *Mechanical Systems and Signal Processing*, 127:120–135, 2019.
[48] Rodrigo Astroza, Hamed Ebrahimian, Yong Li, and Joel P Conte. Bayesian nonlinear structural fe model and seismic input identification for damage assessment of civil structures. *Mechanical Systems and Signal Processing*, 93:661–687, 2017.
[49] Juan Castiglione, Rodrigo Astroza, Saeed Eftekhar Azam, and Daniel Linzell. Auto-regressive model based input and parameter estimation for nonlinear finite element models. *Mechanical Systems and Signal Processing*, 143:106779, 2020.
[50] JN Yang, S Pan, and H Huang. An adaptive extended kalman filter for structural damage identifications ii: unknown inputs. *Structural Control and Health Monitoring: The Official Journal of the International Association for Structural Control and Monitoring and of the European Association for the Control of Structures*, 14(3):497–521, 2007.
[51] Abdullah Al-Hussein and Achintya Haldar. Unscented kalman filter with unknown input and weighted global iteration for health assessment of large structural systems. *Structural Control and Health Monitoring*, 23(1):156–175, 2016.
[52] Kristof Maes, MN Chatzis, and Geert Lombaert. Observability of nonlinear systems with unmeasured inputs. *Mechanical Systems and Signal Processing*, 130:378–394, 2019.
[53] K Maes, MN Chatzis, R Vandebril, and G Lombaert. Observability of modally reduced order models with unknown parameters. *Mechanical Systems and Signal Processing*, 146:106993, 2021.

[54] Qinghua Zhang and Liangquan Zhang. State estimation for stochastic time varying systems with disturbance rejection. *IFAC-PapersOnLine*, 51(15):55–59, 2018.
[55] Subhamoy Sen, Neha Aswal, Qinghua Zhang, and Laurent Mevel. Structural health monitoring with non-linear sensor measurements robust to unknown non-stationary input forcing. *Mechanical Systems and Signal Processing*, 152:107472, 2021.
[56] Ai-Lun Wu, Jann N Yang, and Chin-Hsiung Loh. A finite-element based damage detection technique for nonlinear reinforced concrete structures. *Structural Control and Health Monitoring*, 22(10):1223–1239, 2015.
[57] Siu-Lai Chan and Pui-Tak Chui. *Non-linear static and cyclic analysis of steel frames with semi-rigid connections*. Elsevier, 2000.
[58] Miodrag Sekulovic, Ratko Salatic, and Marija Nefovska. Dynamic analysis of steel frames with flexible connections. *Computers & structures*, 80(11):935–955, 2002.
[59] Bureau Indian Standard. General construction in steel-code of practice. *3rd Revision, Bureau of Indian Standard, New Delhi, India, IS*, pages 800–2007, 2007.
[60] M Soares Filho, MJR Guimarães, CL Sahlit, and JLV Brito. Wind pressures in framed structures with semi-rigid connections. *Journal of the Brazilian Society of Mechanical Sciences and Engineering*, 26(2):174–179, 2004.

Appendix A. Beam element with semi-rigid joint

Traditionally structural joints are idealized with an assumption on the rotational stiffness, i.e., infinite for the fixed joint or zero for the pin joint. For the semi-rigid joint assumption, Eurocode 3 (2003) introduces a factor, called joint stiffness index (γ), to quantify the rotational stiffness, k, of a beam joint as,

$$k = \gamma \frac{E_m I_m}{l_m} \tag{A.1}$$

E_m, I_m and l_m are the modulus of elasticity, moment of inertia along the axis of bending and length of the member, respectively. Nominally, $\gamma \leq 0.5$ is considered for pin joints while $\gamma \geq 8$ (for braced frames) and $\gamma \geq 25$ (for unbraced frames) are considered for rigid joints. For semi-rigid joints, the value of γ lies within the range of $[0.5, 25]$. Eurocode 3 (2003) further defines end fixity factor, P, for a beam joint end as a function of γ as,

$$P = \frac{\gamma}{3+\gamma} \tag{A.2}$$

Thus, for perfectly pinned connection (i.e. $k = 0$) $P = 0$ while for a perfectly rigid connection (i.e. $k = \infty$) $P = 1$. For semi-rigid connection P lies within the range of $[0.143 - 0.893]$.

With this definition of joint stiffness, several studies [1, 7, 60] developed the model of an Euler-Bernoulli beam supported on two semi-rigid joints e and f with end fixity factors P_e and P_f respectively (cf. Figure 1). [1] derived the corresponding elemental stiffness matrix as

$$K^m_{local} = \frac{E_m I_m}{l_m} \begin{bmatrix} \frac{A_m}{I_m} & 0 & 0 & -\frac{A_m}{I_m} & 0 & 0 \\ & \frac{4(\alpha_1+\alpha_2+\alpha_3)}{l_m^2} & \frac{2(2\alpha_1+\alpha_2)}{l_m} & 0 & -\frac{4(\alpha_1+\alpha_2+\alpha_3)}{l_m^2} & \frac{2(2\alpha_2+\alpha_3)}{l_m} \\ & & 4\alpha_1 & 0 & -\frac{2(2\alpha_1+\alpha_2)}{l_m} & 2\alpha_2 \\ & & & \frac{A_m}{I_m} & 0 & 0 \\ & & & & \frac{4(\alpha_1+\alpha_2+\alpha_3)}{l_m^2} & -\frac{2(2\alpha_2+\alpha_3)}{l_m} \\ Sym. & & & & & 4\alpha_3 \end{bmatrix} \tag{A.3}$$

where, A_m is the cross-sectional area of the member and α_1, α_2, and α_3 can be obtained as

$$\alpha_1 = \frac{3P_e}{4 - P_e P_f}, \quad \alpha_2 = \frac{3P_e P_f}{4 - P_e P_f}, \quad \alpha_3 = \frac{3P_f}{4 - P_e P_f}. \tag{A.4}$$

The corresponding elemental mass matrix is defined as

$$M^m_{local} = \frac{\rho l_m}{420D^2} \begin{bmatrix} 140D^2 & 0 & 0 & 70D^2 & 0 & 0 \\ & 4f_1(P_e,P_f) & 2l_m f_2(P_e,P_f) & 0 & 2f_3(P_e,P_f) & -l_m f_4(P_e,P_f) \\ & & 4L^2 f_5(P_e,P_f) & 0 & l_m f_4(P_f,P_e) & -L^2 f_6(P_e,P_f) \\ & & & 140D^2 & 0 & 0 \\ & & & & 4f_1(P_f,P_e) & -2l_m f_2(P_f,P_e) \\ Sym. & & & & & 4L^2 f_5(P_f,P_e) \end{bmatrix} \tag{A.5}$$

where, ρ is the mass per unit length of the member and

$$\begin{aligned} D &= 4 - P_e P_f \\ f_1(P_e,P_f) &= 560 + 224P_e + 32P_e^2 - 196P_f - 328P_e P_f - 55P_e^2 P_f + 32P_f^2 + 50P_e P_f^2 + 32P_e^2 P_f^2 \\ f_2(P_e,P_f) &= 224P_e + 64P_e^2 - 160P_e P_f - 86P_e^2 P_f + 32P_e P_f^2 + 25P_e^2 P_f^2 \\ f_3(P_e,P_f) &= 560 - 28P_e - 64P_e^2 - 28P_f - 148P_e P_f + 5P_e^2 P_f - 64P_f^2 + 5P_e P_f^2 + 41P_e^2 P_f^2 \\ f_4(P_e,P_f) &= 392P_f - 100P_e P_f - 64P_e^2 P_f - 128P_f^2 - 38P_e P_f^2 + 55P_e^2 P_f^2 \\ f_5(P_e,P_f) &= 32P_e^2 - 31P_e^2 P_f + 8P_e^2 P_f^2 \\ f_6(P_e,P_f) &= 124P_e P_f - 64P_e^2 P_f - 64P_e P_f^2 + 31P_e^2 P_f^2. \end{aligned} \tag{A.6}$$

This approach provides the elemental mass (M^m_{local}) and stiffness (K^m_{local}) matrices (cf. Equations A.3 and A.5) for the m^{th} member defined in local coordinate system (LCS). These elemental matrices are further assembled in global coordinate system (GCS) to obtain the global mass ($\mathbf{M}$) and stiffness ($\mathbf{K}$) matrices. For the damping $\mathbf{C}$, Rayleigh model of viscous damping has been assumed.